Luminscent Graphene Quantum Dots for Organic Photovoltaic Devices

6 AUTHORS, INCLUDING:

Neeraj Chaudhary
National Physical Laboratory - India
7 PUBLICATIONS **319** CITATIONS

SEE PROFILE

Ritu Srivastava
National Physical Laboratory - India
109 PUBLICATIONS **934** CITATIONS

SEE PROFILE

Luminscent Graphene Quantum Dots for Organic Photovoltaic Devices

Vinay Gupta,* Neeraj Chaudhary, Ritu Srivastava, Gauri Datt Sharma, Ramil Bhardwaj, and Suresh Chand

Organic and Hybrid Solar Cell Group, National Physical Laboratory, Dr. K. S. Krishnan Marg, New Delhi 110012, India

S *Supporting Information*

ABSTRACT: Recent research in organic photovoltaic (OPV) is largely focused on developing low cost OPV materials such as graphene. However, graphene sheets (GSs) blended conjugated polymers are known to show inferior OPV characteristics as compared to fullerene adduct blended with conjugated polymer. Here, we demonstrate that graphene quantum dots blended with regioregular poly(3-hexylthiophene-2,5-diyl) or poly(2-methoxy-5-(2-ethylhexyloxy)-1,4phenylenevinylene) polymer results in a significant improvement in the OPV characteristics as compared to GSs blended conjugated polymers. This work has implications for inexpensive and efficient solar cells as well as organic light emitting diodes.

The widespread commercialization of conjugated polymer-based organic photovoltaic (OPV) devices remains limited due to the use of high-cost donor and acceptor materials.[1] Therefore, development of new cost-effective materials[2] is critical for the future of OPVs. Quantum dots (QDs) (e.g., CdSe, CdTe, PbTe) are emerging as the leading acceptor materials in photovoltaics[3,4] due to their size-tuned optical response, efficient multiple carrier generation, and low cost.[5] However, their toxicity and hazardous nature are serious impediments for large-scale device applications. Therefore, benign nanomaterials with similar properties are needed. Graphene has been shown to be a good electron acceptor, with mobility as high as 7×10^4 cm^2 V^{-1} s^{-1}. Higher carrier motilities means that charges are transported to respective electrodes more quickly, which reduces current losses via recombination and therefore improves the efficiency of a solar cell.[4-10] However, solar cells based on conjugated polymers/soluble graphene[11-13] or graphene oxide (GO)[13,14] show much inferior characteristics as compared to fullerene acceptor-based solar cells.[1] Theoretical and experimental studies of graphene have indicated that its bandgap and hence optical properties can be manipulated by reducing its size to the nano level.[15-18] Here, we show that a conjugated polymer blended with graphene quantum dot (GQD) acceptors exhibits a significant enhancement in OPV characteristics as compared to the corresponding conjugated polymer-GS blends.

The GQDs were synthesized from GSs by a hydrothermal approach as described elsewhere.[19] In brief, GSs were obtained by thermal oxidation of GO sheets. The GSs were subjected to hydrothermal treatment at 200 °C, followed by a dialysis process. The dialysis process allowed separation of GQDs from larger molecules through a semi-permeable membrane with retained
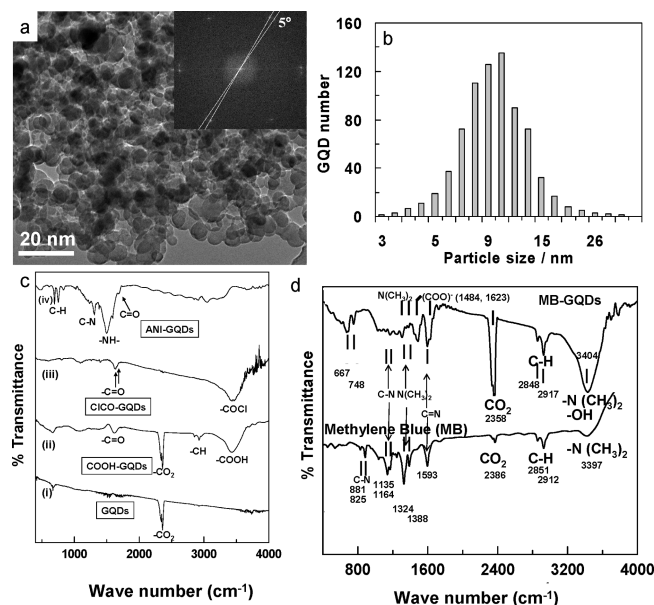

Figure 1. (a) TEM image, (b) diameter distribution, and (c,d) FTIR spectra of the GQDs.

molecular weight of 3500 Da, as shown in Figure S1 of the Supporting Information (SI). The transmission electron microscopy (TEM) image of the synthesized GQDs is shown in Figure 1a. The fast Fourier transform (FFT) of GQDs is shown in the inset of Figure 1a, which confirms that most GQDs consist of 1−2 layers.[20] The particle size distribution measurements of GQDs were performed using a laser scattering particle size analyzer (HORIBA, LB 500X). The sizes were mainly in the range of 5−15 nm (9 nm average), as shown in the Figure 1b. The X-ray diffraction and Raman spectra of GQDs show characteristics of sp^2 carbon (Figure S2 in SI) with disorder due to scattering at the edges.[21]

For solar cell applications, we have functionalized GQDs with aniline (ANI), similar to phenyl isocyanate used in the case of GSs.[11] For organic light emitting diode (OLED) applications, fluorescent dye is often mixed with polymer to make the emitting layer.[22] Here, in order to see the direct effect of GQDs on the performance of poly(2-methoxy- 5-(2-ethylhexyloxy)-1,4phenylenevinylene) (MEH-PPV) polymer, methylene blue (MB) dye is used because it is nonfluorescent (Figure 2b). The method
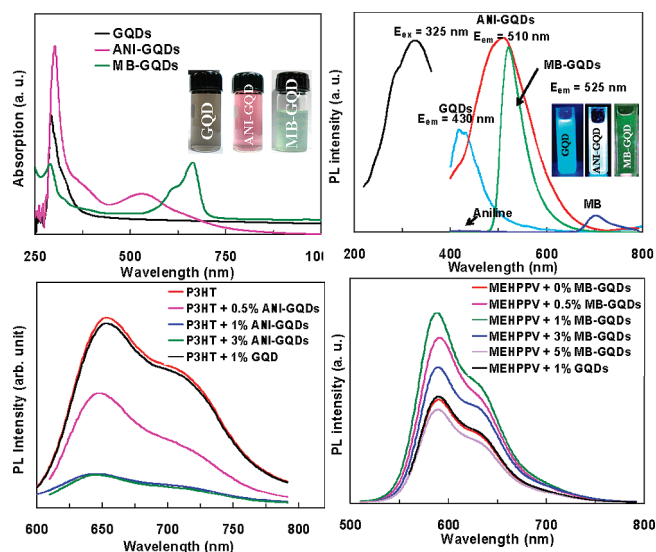
Figure 2. (a) UV−vis absorption, (b) PL spectra of GQDs, ANI-GQDS, MB, Aniline, and MB-GQDs (c) PL spectra of P3HT/ANI-GQDs, and (d) PL spectra of MEH-PPV/MB-GQDs.

of preparation of ANI-GQDs and MB-GQDs is detailed in the SI. In brief, GQDs were first treated in HNO_3 to attach carboxyl groups[23] (carboxylation reaction, scheme 1, SI). The alkyl chloride synthesis method was then followed, in which the carboxylated GQDs were reacted with $SOCl_2$ in the presence of dimethylformamide (catalyst). This resulted in the formation of COCl-GQDs[22,23] (scheme 2, SI). After that, the acylation reaction was followed, in which aniline reacted with acyl chlorides (COCl-GQDs in this case), and C_6H_5-NH-CO-GQD (ANI-GQDs) anilide was formed[23−25] (scheme 3, SI). The same acylation reaction was also used to attach MB to carboxylated GQDs (scheme 4, SI). These surface exchanges were analyzed by Fourier transformed infrared (FTIR) spectroscopy. The FTIR spectrum of GQDs (Figure 1c(i)), after carboxylation (Figure 1c(ii)), confirms the functionalization of GQDs with carboxyl group[23] ($-COOH$, $\nu_{C=O} \approx 1721$ cm^{-1}) and hydroxyl O−H group ($\nu_{O-H} \approx 3423$ cm^{-1}). Further, acylation of the carboxyl group resulted in the splitting of $\nu_{C=O}$ into a doublet[26] ($-COCl$, $\nu_{C=O} = 1731$ and 1772 cm^{-1}), as shown in Figure 1c(iii). The FTIR spectrum of the ANI-GQDs (Figure 1c(iv)) shows a shift of the C=O band to lower frequency ($\nu_{C=O} = 1611-1671$ cm^{-1}),[23,27] which indicates the formation of an amide bond. In addition, the presence of new bands at 1492 and 1308 cm^{-1} corresponding to N−H in-plane and C−N bands,[27] respectively, confirms the amide functionalization. The modification of the FTIR spectra after treatment with MB confirms the formation of MB-GQDs, as shown in Figure 1d. The functionalization of GQDs was corroborated by X-ray photoelectron spectroscopy (Figure S3, SI) Thermogravimetric analysis (Figure S4, SI) showed weight losses of 9.6, 56.6, and 62.9% for COOH-GQDs, ANI-GQDs, and MB-GQDs, respectively, which also confirms the functionalization of GQDs.[11,12]

The UV−vis absorption spectra and the optical images of GQDs, ANI-GQDs, and MB-GQDs (in ethanol) are shown in Figure 2a. The spectrum of GQDs shows typical absorption peaks at 292 and 325 nm, which are very different from the GSs peaks at ca. 230 nm due to $\pi \rightarrow \pi^*$ transition of aromatic sp^2 domains.[19] The two electronics transitions of 325 nm (3.81 eV)

and 292 nm (4.24 eV) observed in the photoluminescence (PL) spectrum of GQDs can be regarded as transitions from σ and π orbitals, viz. highest occupied molecular orbital (HOMO) to lowest unoccupied molecular orbital (LUMO).[19,28] The UV−vis absorption spectra of pure aniline and MB are shown in Figure S5 (SI). The UV−vis spectrum of ANI-GQDs (Figure 2a) gives a broad absorption peak in the visible region centered at ∼525 nm, which extends to 800 nm, and its color is pink. The UV−vis spectrum of MB-GQDs is narrow, and its color is green (Figure 2a). Both aniline and MB do not show any detectable PL in the visible region (Figure 2b). The PL emission of GQDs (excitation wavelength $E_{ex} = 325$ nm) appears at 430 nm,[13] giving blue luminescence (inset of Figure 2b).[19] The PL spectrum of the GQDs changes significantly after functionalization. The PL spectrum of ANI-GQDs (Figure 2b) is extended from 400 to 700 nm (centered at 510 nm); hence, the luminescence is changed from blue to white (inset of Figure 2b). The PL spectrum of MB-GQDs (475−700 nm) is narrow (Figure 2b) and extended from 475 to 700 nm (centered at 525 nm), giving green luminescence (inset of Figure 2b). The origin of PL in graphene depends on the chemical nature of the graphene edges, which is explained in detail by Radovic et al.[28] They proposed that the zigzag edges sites of graphene are carbine-like, with the triplet ground state being most common. Not only is this proposal consistent with the key electronic properties and surface (re)activity behavior of carbons,[28] but it can also explain the enhanced PL (Figure 2) in GQDs,[19] PEG-ylated nano graphene oxide,[29] CNTs,[30] and carbon nanoparticles.[31]

The PL emission spectra ($E_{ex} = 510$ nm) of the films of poly(3-hexylthiophene-2,5-diyl) (P3HT) blended with ANI-GQDs in different wt % ratios (0, 0.5, 1, 3, 5 wt %) are shown in Figure 2c. The PL shows quenching behavior with saturation at 1 wt % ANI-GQDs. In comparison, 1 wt % of nonfunctionalized GQDs do not show any quenching effect. Among the three mechanisms for PL quenching, namely energy transfer, exciplex formation, and charge transfer, only the excited-state charge transfer (CT) can account for the PL quenching of P3HT because of the absence of additional spectral features in the PL spectra of the blends as compared to P3HT. In the CT process, the photo-induced excitons generated in P3HT are dissociated at the heterojunction interface between P3HT and ANI-GQDs, which leads to a nonradiative relaxation of the excitons. The PL emission spectra ($E_{ex} = 450$ nm) of the films of MB-GQDs blended with MEH-PPV in different wt % ratios (0, 0.5, 1, 3, 5 wt %) are shown in Figure 2d. The PL emission of MEH-PPV shows an intense peak at 590 nm accompanied by a shoulder located at 640 nm. Also there is no new peak with the addition of MB-GQDs. As the MB-GQDs is added, the PL intensity of MEH-PPV is increased, and after 1 wt % of MB-GQDs the PL intensity is decreased. At low concentrations, the enhancement in the PL intensity is been attributed to an energy transfer from GQDs to the MEH-PPV matrix, and after an optimum concentration the energy transfer is from MEH-PPV to GQDs, which results in quenching. As we increase the concentration of GQDs, their agglomeration takes place, and because of agglomeration, phase separation takes place. In comparison, 1 wt % of nonfunctionalized GQDs do not show any quenching effect at all due to ineffective blending, as discussed later. It is seen that the photoemission of the blended film exhibits much higher luminescence intensity for 0.5−3 wt % of MB-GQDs than that of the pure MEH-PPV.

Quantitative PL intensity measurements, however, depend crucially on the alignment and illumination geometry, and in the
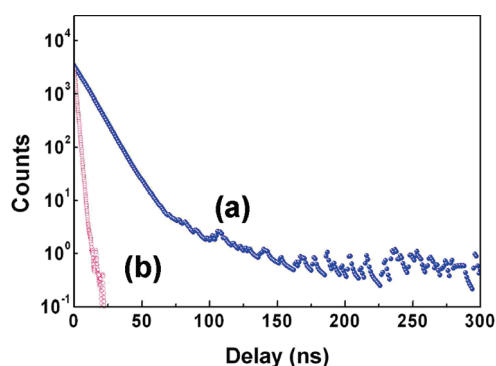
Figure 3. Time resolved PL spectra of P3HT/ANI-GQDs and P3HT/MB-GQDs co-casting films excited at 510 nm.

Table 1. Performance Details (V_{oc}, J_{sc}, FF and η) of the P3HT/ANI-GQDs and P3HT/ANI-GSs under Simulated AM 1.5G 100 mW Illumination

type of graphene	graphene wt %	V_{oc} [V]	J_{sc} [mA cm^{-2}]	FF	η [%]
—	0	0.43	0.037	0.21	0.003
ANI-GQDs	*0.5*	*0.62*	*2.65*	*0.47*	*0.77*
ANI-GSs	0.5	0.71	0.15	0.19	0.02
ANI-GQDs	*1*	*0.61*	*3.51*	*0.53*	*1.14*
ANI-GSs	1	0.72	0.19	0.22	0.03
ANI-GQDs	*3*	*0.58*	*1.32*	*0.51*	*0.39*
ANI-GSs	3	0.86	0.55	0.27	0.13
ANI-GQDs	*5*	*0.59*	*0.36*	*0.52*	*0.12*
ANI-GSs	5	0.94	1.5	0.33	0.46
ANI-GSs	10	0.88	2.65	0.28	0.65
ANI-GSs	15	0.95	0.31	0.25	0.07

case of films it should also reflect the local morphology. Co-casting of P3HT and ANI-GQDs as well as MB-GQDs could very well influence the film morphology, leading to different and spatially varying P3HT concentrations. To ascertain quenching or radiative rate modifications, the excited-state dynamics of P3HT/1 wt % ANI-GQDs (Figure 3a) and P3HT/MB-GQDs (1 wt %) (Figure 3b) were measured by time-resolved PL spectroscopy. The contrasting PL decay behavior of ANI-GQDs and MB-GQDs is quite evident as PL decay of the P3HT/MB-GQDs (1 wt %) ($\tau \approx 10^{-10}$ s) is an order of magnitude faster than that of the P3HT/ANI-GQDs (1 wt %) ($\tau \approx 10^{-9}$ s).

P3HT/ANI-GQD-based hybrid solar cells were fabricated by spin-casting a solution of 15 mg mL^{-1} P3HT in dichlorobenzene (DCB) with ANI-GQDs contents of 0.5, 1, 3, and 5 wt % (ratio to P3HT) onto indium tin oxide (ITO), coated with poly(ethylene dioxythiophene)−polystyrene sulfonic acid (PEDOT:PSS) conductive polymer, which acted as the bottom electrode. LiF and Al were then vacuum deposited as the top contact (Figure S6 in SI) to form an OPV device having the structure ITO/PEDOT:PSS/P3HT:ANI-GQDs/LiF/Al.[11] For comparison, the solar cells of P3HT/ANI-GSs with ANI-GSs contents of 0.5, 1, 3, 5, 10, and 15 wt % (ratio to P3HT) were also fabricated. The solar cell characteristics were measured under 100 mW AM 1.5G illumination. The obtained power conversion efficiency (η), open-circuit voltage (V_{oc}), short-circuit current density (J_{sc}), and fill factor (FF) are summarized in Table 1. It can be seen that the FF of the P3HT/ANI-GQDs hetrojunction device is much higher (0.53)
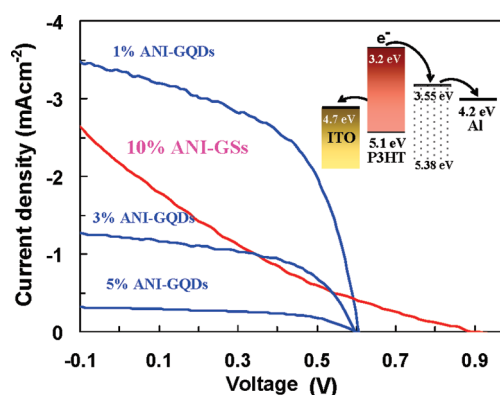

Figure 4. $J-V$ characteristics of the photovoltaic devices based on ANI-GQDs with different GQDs content and ANI-GS (under optimized condition) annealed at 160 °C for 10 min, in AM 1.5G 100 mW illumination.
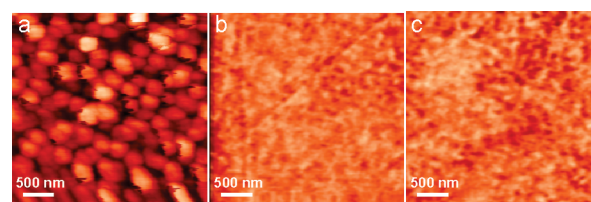

Figure 5. AFM images of (a) P3HT/ANI-GSs, (b) P3HT/ANI-GQDs, and (c) MEH-PPV/MB-GQDs.

as compared to ∼0.33 for GSs.[11,12] Current density versus voltage ($J-V$) curves of the ANI-GQD and ANI-GS (optimized) PV devices are plotted in Figure 4. The corresponding band diagram is given in the inset of Figure 4. Maximum values of $\eta = 1.14$, $V_{oc} = 0.61$ V, $J_{sc} = 3.51$ mA cm^{-2}, and FF = 0.53 were obtained for 1 wt % ANI-GQD in P3HT. In comparison, maximum values of $\eta = 0.65$, $V_{oc} = 0.88$ V, $J_{sc} = 2.65$ mA cm^{-2}, and a low FF = 0.28 were obtained for 10 wt % ANI-GSs in P3HT, similar to those reported earlier.[11,12] The corresponding band diagram is shown in the inset of Figure 4. The LUMO and HOMO of GQDs, determined by cyclic voltammetry (CV),[32] were −3.55 and −5.38 eV, respectively (Figure S7, SI). The position of the LUMO (or work function) of GQDs between those of P3HT[1] and Al suggests their suitability for OPV applications.

Since the photocurrent is mostly limited by photoinduced charge carrier generation and transport, the nanoscale morphology of the P3HT/ANI-GQDs blend film is an important factor for the determining the value of FF. The atomic force microscopy (AFM) image of the P3HT/ANI-GSs film (Figure 5a) shows that there are large domains (about 100−200 nm diameter), indicating large-scale phase separation and much larger than the diffusion length of excitons (10 nm), whereas the AFM image of P3HT/ANI-GQD shows uniform and fine features, suggesting nanoscale phase separation. This results in enhancement of the exciton migration to the donor/acceptor interface, resulting in a decrease in the resistance and a corresponding increases in the FF. So the improved morphology of the P3HT/ANI-GQD results in improved performance of the solar cell.

OLED devices were fabricated under the optimized condition from MEH-PPV, MEH-PPV/GQDs(1%), and MEH-PPV/MB-GQDs(1%) solution in DCB by a process similar to that used for a solar cell device, i.e. ITO/PEDOT:PSS/MEH-PPV:MB-GQDs/LiF/Al (Figure S8, SI). Figure 6 shows the $J-V$ curves of
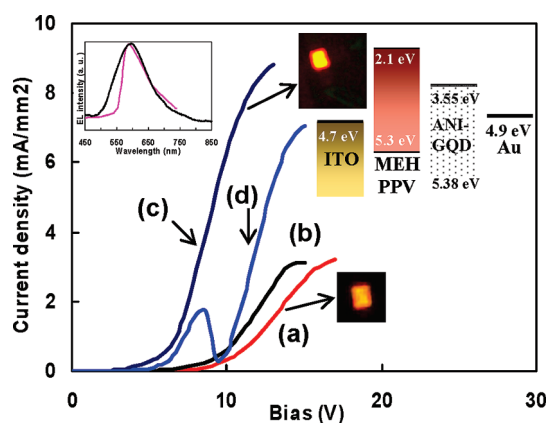
Figure 6. Measured current density of MEH-PPV with MB-GQDs (a) 0%, (b) 0.5%, (c) 1%, and (d) 3% as a function of the applied voltage (*V*). The inset plots the electroluminescence spectrum of the MEH-PPV (red) and MEH-PPV/MB-GQDs (1%) (black). The inset also shows the band diagram of the MEH-PPV/MB-GQDs and the recorded brightness of MEH-PPV LED and MEH-PPV/MB-GQDs (1%) LED.

the different OLEDs. The corresponding band diagram is given in the inset of Figure 6. The turn-on voltage for the pure MEH-PPV sample (Figure 6a) is ∼6 V and is decreased to ∼4 V for MEH-PPV/MB-GQDs(1%) (Figure 6c). At higher concentration (3% MB-GQDs), charge trapping as well as a shortening effect is observed, possibly due to agglomeration (Figure 6d). The enhancement of the maximum light-emission intensity after blending MEH-PPV with MB-GQDs directly reflects the enhanced efficiency. MEH-PPV/MB-GQDs(1%) exhibits strong yellow emission, as compared to the bright orange emission of MEH-PPV. The inset of Figure 6 shows the corresponding electroluminescence (EL) spectra. The EL spectrum of MEH-PPV/MB-GQDs(1%) starts from lower wavelength as compared to MEH-PPV. The MB-GQDs dispersed in the MEH-PPV provides more electrical transport paths, which results in an enhancement of charge injection and hence causes increase in the carrier density, thus requiring lower turn-on voltage and much higher efficiency. The AFM image of MEH-PPV/MB-GQDs (Figure 5c) also shows that the film has uniform and fine features.

In conclusion, we have demonstrated that the GQDs dispersed in conjugated polymers show enhanced OPV and OLED characteristics as compared to GSs due to improved morphological and optical characteristics. The performance of GQD-based devices can be further improved by choosing other polymers or different types of functionalization. GQDs can be a cost-effective, environmentally friendly, and more stable material for photovoltaics than current organic materials.

■ ASSOCIATED CONTENT

ⓢ Supporting Information. Detailed characterization of GQDs, ANI-GQDs, and MB-GQDs; UV–vis spectra of anilne and MB. This material is available free of charge via the Internet at http://pubs.acs.org).

■ AUTHOR INFORMATION

Corresponding Author
drvinaygupta@netscape.net

■ REFERENCES

(1) Kim, J. Y.; Lee, K.; Coates, N. E.; Moses, D.; Nguyen, T.-Q.; Dante, M.; Heeger, A. J. *Science* **2007**, *317*, 222–225.

(2) Li, C.; Liu, M.; Pschirer, N. G.; Baumgarten, M.; Müllen, K. *Chem. Rev.* **2010**, *110*, 6817–6855.

(3) Huynh, W. U.; Dittmer, J. J.; Alivisatos, A. P. *Science* **2002**, *295*, 2425–2427.

(4) Jaiswal, J. K.; Goldman, E. R.; Mattoussi, H.; Simon, S. M. *Nat. Methods* **2004**, *1*, 73–78.

(5) Castro Neto, A. H.; Guinea, F.; Peres, N. M. R.; Novoselov, K. S.; Geim, A. K. *Rev. Mod. Phys.* **2009**, *81*, 109–162.

(6) Geim, A. K.; Novoselov, K. S. *Nat. Mater.* **2007**, *6*, 183–191.

(7) Geim, A. K. *Science* **2009**, *324*, 1530–1534.

(8) Castro Neto, A. H.; Guinea, F.; Peres, N. M. R.; Novoselov, K. S.; Geim, A. K. *Rev. Mod. Phys.* **2009**, *81*, 109–162.

(9) Pisula, W.; Feng, X.; Müllen, K. *Chem. Mater.* **2011**, *23*, 554–567.

(10) Wang, X.; Zhi, L.; Tsao, N.; Željko, T.; Li, J.; Müllen, K. *Angew. Chem. Int. Ed.* **2008**, *41*, 2990–2992.

(11) Liu, Z.; Liu, Q.; Huang, Y.; Ma, Y.; Yin, S.; Zhang, X.; Sun, W.; Chen, Y. *Adv. Mater.* **2008**, *20*, 3924–3930.

(12) Liu, Q.; Liu, X.; Zhang, X.; Yang, L.; Zhang, N.; Pan, G.; Yin, S.; Chen, Y.; Wei, J. *Adv. Funct. Mater.* **2009**, *19*, 894–904.

(13) Yu, D.; Yang, Y.; Durstock, M.; Baek, J.-B.; Dai, L. *ACS Nano* **2010**, *4*, 5633–5640.

(14) Hill, C. M.; Zhu, Y.; Pan, S. *ACS Nano* **2011**, *2*, 942–951.

(15) Müller, M. M.; Yan, X.; McGuire, J. A.; Li, L.-S. *Nano Lett.* **2010**, *10*, 2679–2682.

(16) Huang, B; Yan, Q. M.; Li, Z. Y.; Duan, W. H. *Front. Phys. China* **2009**, *4*, 269–279.

(17) Yan, X.; Cui, B.; Li, L.-S. *J. Am. Chem. Soc.* **2010**, *132*, 5944–5945.

(18) Yan, X.; Cui, B.; Li, L.-S. *Nano Lett.* **2010**, *10*, 1869–1873.

(19) Pan, D.; Zhang, J.; Li, Z.; Wu, M. *Adv. Mater.* **2010**, *22*, 734–738.

(20) Ci, L.; Song, L.; Jin, C.; Jariwala, D.; Wu, D.; Li, Y.; Srivastava, A.; Wang, Z. F.; Storr, K.; Balicas, L.; Liu, F.; Ajayan, P. M. *Nat. Mater.* **2010**, *9*, 430–435.

(21) Ferrari, A. C.; Meyer, J. C.; Scardaci, V.; Casiraghi, C.; Lazzeri, M.; Mauri, F.; Piscanec, S.; Jiang, D.; Novoselov, K. S.; Roth, S.; Geim, A. K. *Phys. Rev. Lett.* **2006**, *97*, 187401.

(22) Matyba, P.; Yamaguchi, H.; Eda, G.; Chhowalla, M.; Edman., L.; Robinson, N. D. *ACS Nano* **2010**, *4*, 637–642.

(23) Santoro, G. E.; Martoňák, R.; Tosatti, E.; Car, R. *Science* **2002**, *295*, 2425–2427.

(24) http://en.wikipedia.org/wiki/Acyl_chloride

(25) http://en.wikipedia.org/wiki/Aniline

(26) Hung, N. T.; Anoshkin, I. V.; Dementjev, A. P.; Katorov, D. V.; Rakov, E. G. *Inorg. Mater.* **2008**, *44*, 219–223.

(27) Ramathan, T.; Fisher, F. T.; Ruoff, R. S.; Brinson, L. C. *Chem. Mater.* **2005**, *17*, 1290–1295.

(28) Radovic, L. R.; Bockrath, B. *J. Am. Chem. Soc.* **2005**, *127*, 5917.

(29) Liu, Z.; Robinson, J. T.; Sun, X.; Dai, H. *J. Am. Chem. Soc.* **2008**, *130*, 10876–10877.

(30) Zhou, J.; Booker, C.; Li, R.; Zhou, X.; Sham, T.-K.; Sun, X.; Ding, Z. *J. Am. Chem. Soc.* **2007**, *129*, 744–745.

(31) Pan, D.; Zhang, J.; Li, Z; Wu, C.; Yana, X.; Wu, M. *Chem. Commun.* **2010**, *46*, 3681–3683.

(32) Admassie, S.; Inganäs, O; Mammo, W.; Perzon, E.; Andersson., M. R. *Synth. Met.* **2006**, *156*, 614–623.

9963

dx.doi.org/10.1021/ja2036749 |*J. Am. Chem. Soc.* 2011, 133, 9960–9963